

## COLLISIONS BETWEEN HIGH-LATITUDE CLOUDS: THEORY MEETS OBSERVATIONS

E. R. KETO AND J. C. LATTANZIO

Institute of Geophysics and Planetary Physics, Lawrence Livermore National Laboratory

Received 1988 December 12; accepted 1989 April 24

### ABSTRACT

We report on fully three-dimensional hydrodynamic and radiative transfer simulations of collisions between high-latitude clouds. Our model uses the smoothed particle hydrodynamics code described by Lattanzio and Henriksen to compute the velocity and density fields in the impacted clouds and a recently developed radiative transfer code to compute  $^{13}\text{CO}$  line radiation from the simulated source. By including the instrumental effects involved in a particular observation we can make detailed comparisons with the observations. The model shows that (1) The previously unexplained energy source for the broad CO line wings reported by Blitz, Magnani, and Wandel derives from the collisions. (2) Collisions can induce rapid gravitational collapse and star formation in these clouds which are otherwise supported against gravitational contraction via their internal energy content. (3) The external pressure due to intercloud H I, first proposed for these objects by Keto and Myers, plays a significant role in the stability and evolution of the high-latitude clouds.

*Subject headings:* hydrodynamics — interstellar: matter — radiation transfer

### I. INTRODUCTION

Broad CO line wings have been recently reported in a few "high-latitude clouds" by Blitz, Magnani, and Wandel (1988, hereafter BMW). The extent of the wings of several  $\text{km s}^{-1}$  is significantly higher than the FWHM of the CO lines, suggesting that the driving energy of the flows must come from some source other than the turbulent motions within the clouds. However, these clouds are devoid of stars and no other internal energy source is known. In this paper we explore the suggestion made independently by BMW, Elmegreen (1988) and Lattanzio and Henriksen (1988, hereafter LH) that cloud collisions may be responsible for the observed high-velocity flows and broad line wings.

The high-latitude clouds as a class have number densities one order of magnitude less than dark clouds and a factor of 5 greater than H I clouds. Their name derives from the fact that they are commonly observed at high Galactic latitude where they can be more easily distinguished from background emission in the Galactic plane. However, they do not differ substantially in observed properties from small diffuse clouds seen closer to the Galactic plane. Much of the observational evidence points to pervasive collisions and shocks in the high-latitude cloud complexes. (1) The velocities implied by the extent of the wings are nearly the same as the velocity dispersion of  $5 \text{ km s}^{-1}$  for individual clouds in typical complexes. (2) Molecular abundances in the high-latitude clouds are similar to abundances thought to be produced by nondissociative shocks (Magnani, Blitz, and Wouterloot 1987). (3) The clumpiness of the interstellar medium may be a reflection of collision morphology: localized zones of compressed gas at the collision contacts surrounded by diffuse high-velocity ejecta. (4) The long filaments of molecular gas observed at high Galactic latitude (de Vries, Heithausen, and Thaddeus 1987) are similar in shape to the flattened structures produced in collisions (see Lattanzio *et al.* 1985, hereafter LMPS). (5) The high-latitude clouds are generally clustered in complexes in which the separation between individual clouds is of the same size scale as the clouds themselves. Thus collisions should be common. Magnani *et al.* (1989) estimate a time between collisions of  $10^4$  yr versus a cloud lifetime of more than  $10^6$  yr.

We use three-dimensional hydrodynamic and radiative transfer simulations to show that the observed spectra can indeed be derived from collisions between high-latitude clouds. The simulations show that for orientations where the cloud velocity field is approximately symmetric with respect to the observer, nearly Gaussian and symmetric profiles will be seen. Strongly asymmetric profiles will be seen off the collision center where a rapidly moving portion of one of the clouds is blended within the observing beam with the denser, low-velocity, postshock gas brought to rest at the cloud interface. Because the line shapes vary with position and orientation, the strong wings may appear localized within an area smaller than the extent of the combined postcollision object.

In the following sections we briefly describe the relevant physics and the numerical methods and relate our chosen initial conditions to the observed properties of high-latitude clouds. We then present a detailed comparison of our simulated spectra with the available observations and characterize the line shapes with respect to the nature of the collisions. Last, we discuss the evolution of the high-latitude clouds. We suggest that collisions may induce gravitational instability and rapid collapse in the postcollision cloud whereas the individual clouds were previously in quasi-equilibrium with their internal energy balanced by self-gravity and the external pressure of the surrounding H I gas. The calculations confirm the suggestion first made by Keto and Myers (1986) that the external pressure of the intercloud medium plays a significant role in the stability and evolution of the high-latitude clouds.

### II. HYDRODYNAMICS

The collisions were calculated with the same code as used by LH with one improvement. In previous calculations the gravitational potential has been found by placing a cubic grid over the matter and solving for the potential on this grid (in fact, a multigrid algorithm is used as described in Monaghan and Lattanzio 1985 and Monaghan and Varnas 1987). In the present version of the code we have replaced this cubic grid with a parallelepiped with the three axial ratios chosen so that the grid just covers the matter in each direction (Lattanzio and Monaghan 1989). With the triaxial multigrid, if the two clouds

collide to form a disk, our new potential solver will quickly obtain the potential only within the disk. This enables us to improve the resolution for a given cost in either computer time or memory.

Based on the sample of high-latitude clouds observed by Magnani, Blitz, and Mundy (1985, hereafter MBM) and Keto and Myers (1986), we adopt the following initial parameters for a typical high-latitude cloud;  $M = 100 M_{\odot}$ ,  $\log n(\text{H}_2) = 2.5$   $\text{cm}^{-3}$ ,  $\mu = 2.33$  amu,  $R = 1.1$  pc,  $T = 80$  K. This temperature is about a factor of 8 higher than indicated by observational evidence. Such a relatively large temperature was chosen for two reasons. (1) The higher temperature increases the sound speed, and thus reduces the Mach number of the collision, and consequently places a less severe demand on the artificial viscosity. (2) The high-latitude clouds have observed FWHM line widths of  $\sim 1$   $\text{km s}^{-1}$ , implying internal energies due to turbulent motions significantly higher than their thermal energies. Our model clouds with their artificially high temperatures plus a modest rotational component described below have internal energies approximately equal to those inferred from the line widths. The assumption of isothermality and the choice of temperature are not critical to our results. First, the observations do not have sufficient resolution to observe the high-temperature gas in the thin postshock layer, nor does our numerical model which is closely matched in resolution to the observations. Second, for optically thin emission, the temperature will enter only as a scaling factor in the emission line strength.

Our clouds are initially spherical and have constant density. Thus  $\alpha = E_{\text{th}}/|E_{\text{gr}}| = 1.826$ . We have approximated the effects of an external medium with constant pressure in the same way as LMPS and have chosen the external pressure as  $P_e/k = 1.6 \times 10^3$   $\text{K cm}^{-3}$  (Keto and Myers 1986). Note that the internal pressure  $P \approx 16P_e$ . To simulate the internal velocity dispersion observed in high-latitude clouds we have used solid-body rotation with  $\Omega = 1.73 \times 10^{-14}$   $\text{s}^{-1}$ . This gives  $\beta = E_{\text{rot}}/|E_{\text{gr}}| = 0.291$  and corresponds to a rotation velocity of  $0.85c$  at the cloud edge, where  $c$  is the adiabatic sound speed. We have taken the relative velocity of the colliding clouds from the observed velocity dispersion of individual clouds within a typical complex as defined by MBM. In the particular cases we consider  $v_{\text{rel}} = 4$   $\text{km s}^{-1}$  or  $5.8c$ . Thus the observable effects of the rotation velocity will be small. In fact, we show below that the broad wings seen in the spectra are due to a combination of bulk motion and projection effects. Finally we define a characteristic time for an individual cloud as  $t_c = (R^3/GM)^{1/2} \approx 1.7 \times 10^6$  yr.

We will discuss at length only two collisions between identical clouds as just defined. The spin angular momenta are perpendicular to the direction of relative motion and mutually antiparallel (see § 5.2 of LH). In case 1 the collision is head-on, and in case 2 the impact parameter is  $b = R$  (the spin-orbital angular momentum is “mixed” in the notation of LH). We used 7132 particles in case 1 and 25,412 in case 2. Additionally, both cases were run with varying resolution, and it was found that neither the hydrodynamics nor the radiative transfer was strongly dependent on the resolution.

For case 1 the evolution is qualitatively similar to sequence 7 in LMPS. After the initial compression into a disk, the clouds reexpand along the direction of relative motion while contracting in the plane of the disk. Figure 1a shows the velocity field in a plane through the center of the object at  $t = 0.381t_c$  since contact, and Figure 1b shows the density contours for  $t =$

$0.996t_c$ . Despite the re-expansion along the direction of relative motion the contraction in the plane of the disk causes the maximum density to continually increase. For the configuration shown in Figure 1a the maximum density is  $18\rho_0$ , where  $\rho_0$  is the initial density. Calculations were stopped at the configuration in Figure 1b, by which time the maximum density is  $40\rho_0$ . We shall refer to the case 1 model at the time of Figure 1a as model A, and Figure 1b as model B. (This evolution will be considered in more detail in § Vd.)

Case 2 is identical except for the nonzero impact parameter. In this case the compression results in a maximum density of  $\sim 10\rho_0$ , but the subsequent re-expansion leads to dissipation of the clouds. Figure 2 shows case 2 at a time of  $0.444t_c$  after contact. We shall call this model C.

Having constructed the models, we still face ambiguity concerning their orientation on the sky. To address this we have taken models A, B, and C and performed six rotations of each. For a representative angle we have arbitrarily chosen  $54^\circ$ . Each rotation is defined by three Euler angles  $\phi$ ,  $\theta$ , and  $\psi$  (Goldstein 1972). The six chosen rotations are given in Table 1. After each rotation, the new  $z$ -axis is the line of sight. Figures 3a and 3b show the original orientation of the colliding clouds and the six line-of-sight directions. We shall refer to the resulting 18 configurations as A1–A6, B1–B6, and C1–C6. Figure 1a shows A1 with the  $z$ -axis as the line of sight; Figure 1b shows B1, and Figure 2 shows C1.

### III. RADIATIVE TRANSFER

We have chosen to model  $^{13}\text{CO}(J = 1 \rightarrow 0)$  which has an optical depth less than 0.2 in typical high-latitude clouds. This allows us to use the optically thin approximation to determine the level populations given the temperature, density, and velocity fields as a result of the SPH calculation. We can then determine the line brightness as a function of frequency and position by integrating the source function along the line-of-sight direction through each grid point. (The code will be more fully described in an upcoming paper; Keto 1989). The resulting image is then convolved with an appropriate instrumental response function and transferred into the AIPS image processing environment (developed by the National Radio Astronomy Observatory) where all the tasks necessary for image display may be handled by the existing software. Thus, one AIPS spectral line data set is produced for each of the six orientations of each of the three models.

The 7132 and 25,412 SPH particles were interpolated onto a cubic grid of size  $h$  for run 1 and  $1.5h$  for run 2, resulting in  $\sim 45^3$  and  $39^3$  grid cells, respectively. For a cloud radius of 1.1 pc this gives a pixel size of 0.046 pc and 0.052 pc or 1:6 and 1:8 at a distance of 100 pc. We used 64 channels to cover the full range of line-of-sight velocities in the output of the SPH model. Since our clouds have a relative velocity of 4  $\text{km s}^{-1}$ , the

TABLE 1  
EULER ANGLES USED IN MODELS

Model Number	$\phi$	$\theta$	$\psi$
1.....	$0^\circ$	0	0
2.....	0	54	0
3.....	54	54	0
4.....	90	90	0
5.....	0	90	0
6.....	rotation 5 followed by 2		

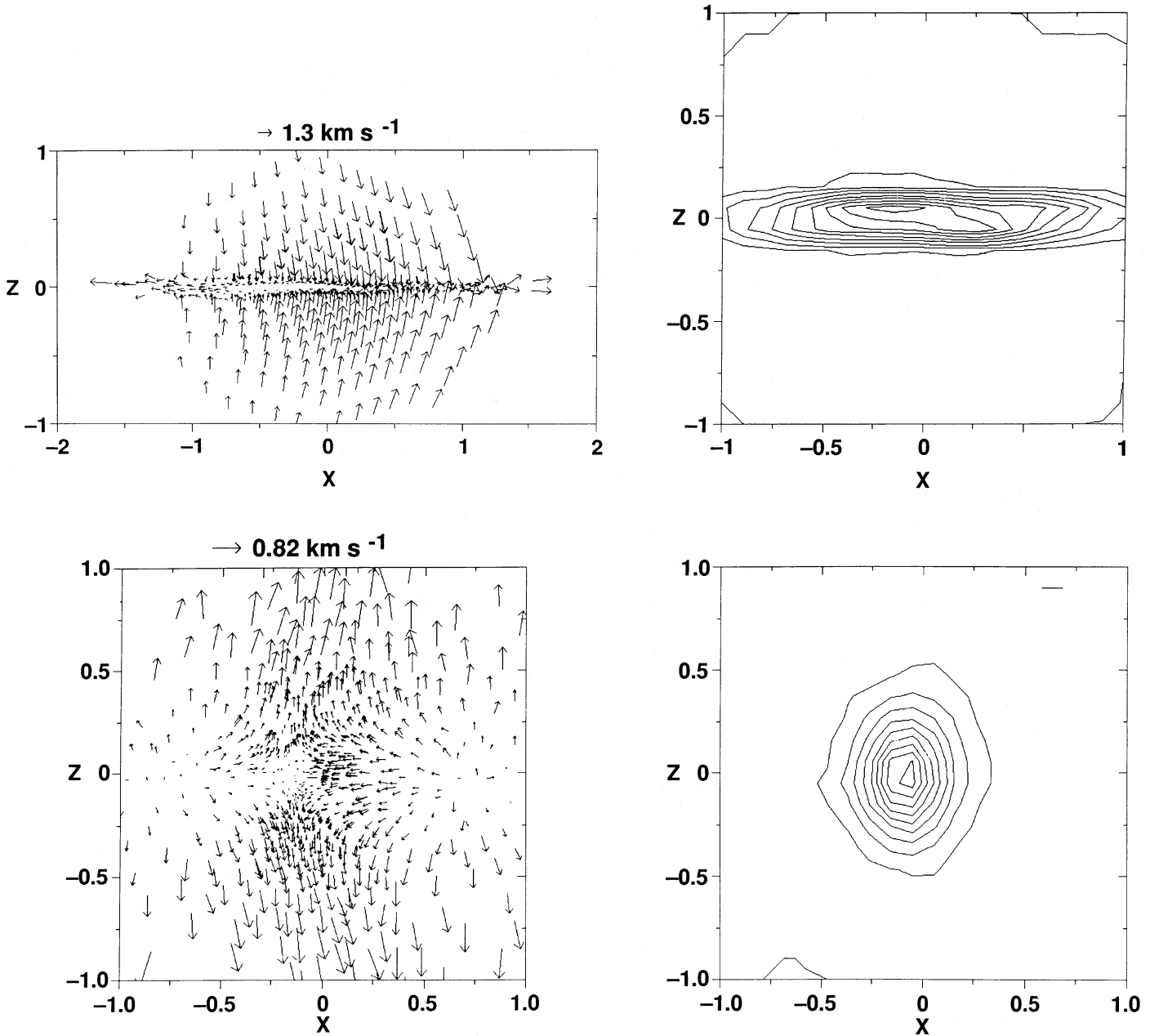


FIG. 1.—Velocity field (left) and density contours (right) for case 1 for two times (a, top; b, bottom) in the  $x, z$  plane through the cloud center. The length unit is 1.1 pc, and  $h$ , the resolution length, is 0.071 for (a) and 0.079 for (b). The density contour interval is  $2.03 \times 10^{-21} \text{ g cm}^{-3}$  for (a) and  $4.88 \times 10^{-21} \text{ g cm}^{-3}$  for (b). The time is  $0.381t_c$  for (a) and  $0.966t_c$  for (b).

typical velocity grid is  $0.06 \text{ km s}^{-1}$ , but varies somewhat with the orientation of the colliding clouds. Estimates of the ratio of  $^{13}\text{CO}$  to  $\text{H}_2$  for high-latitude clouds are  $1 \times 10^{-6}$  (Keto and Myers 1986) and  $1 \times 10^{-6}$  to  $1 \times 10^{-7}$  (Magnani, Blitz, and Wouterloot 1988 and references therein). Using the higher estimate our typical  $^{13}\text{CO}$  line brightness is 0.5 K.

In comparing our  $^{13}\text{CO}$  model spectra with  $^{13}\text{CO}$  and  $^{12}\text{CO}$  spectra from BMW two points should be noted. The comparison of  $^{12}\text{CO}$  and  $^{13}\text{CO}$  data is necessary for two reasons: the paucity of  $^{13}\text{CO}$  spectra at very high signal to noise necessary to detect the low-level wings, and the difficulty of determining accurate population levels in optically thick gas where trap-

ping and radiative excitation may be important. Second, because the  $60''$  observing beam used by BMW is small compared to the  $1^\circ$  extent of the typical high-latitude cloud, we are not able to image an entire cloud at a resolution finer than the observations and convolve the image back to the correct resolution as would be most appropriate. Instead, our grid size is comparable to the resolution of the observations; we have convolved our maps with a 2 pixel Gaussian beam to smooth our computed image over adjacent pixels. Similarly, our initial velocity grid is approximately the same as used in the observations. We have averaged adjacent velocity channels by Hanning smoothing.

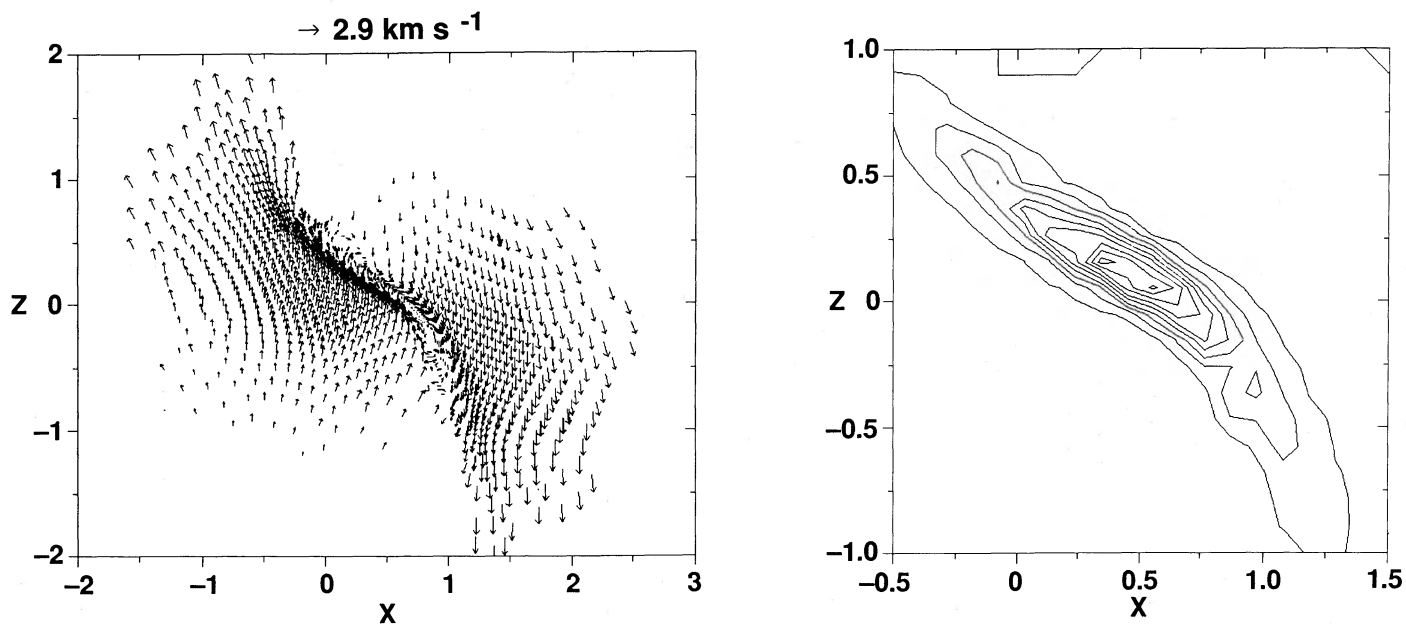


FIG. 2.—Same as Fig. 1, but for case 2. The contour interval is  $1.67 \times 10^{-21} \text{ g cm}^{-3}$ ,  $h = 0.107$ ,  $t = 0.493tc$ .

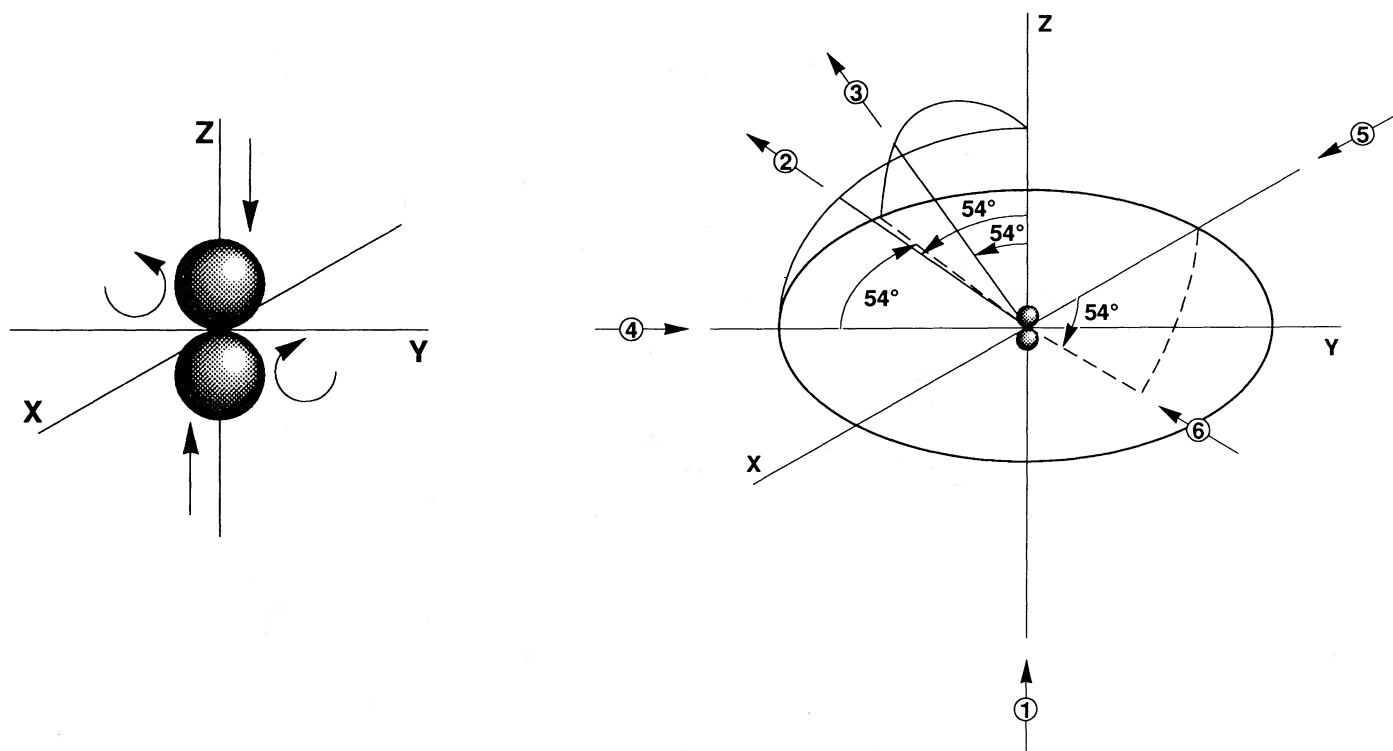


FIG. 3.—(a) Original orientation of the colliding clouds. The relative velocity is along the z-axis. The spin vectors are antiparallel along the y-axis. (b) Orientations of the six line of sight vectors through the model depicted in Fig. 3a. The Euler angles for the six orientations are listed in Table 1. For orientations 1, 4, 5, and 6 the observer looks along the direction indicated by the inward pointing arrows. The observer is to the lower right for orientations 2 and 3, but the vectors have been drawn pointing outward for clarity.

## IV. COMPARISON WITH OBSERVATIONS

Figures 4–6 show the output of the radiative transfer code for three models displayed as the integrated intensity,  $\Sigma I/n$ , and the average line-of-sight velocity  $\Sigma I v/\Sigma I$ , where  $I$  is the line brightness and  $n$  is the number of velocity channels. By comparing the integrated intensity and average velocity maps, one can see that except for the off-axis collision model, where the result appears as two separate clouds, the brightest emission shows very little velocity structure. This is because the densest portion of the cloud, where the collisionally excited CO emits most strongly, is found where the contact between the two colliding clouds has brought the gas nearly to rest (locally). This velocity structure is consistent with observations of high-latitude clouds, which like molecular clouds in general, often show multiple components, but do not show large velocity gradients across simple structures.

In Figure 7 we plot spectra computed at every other position across the entire cloud of model C1. Note how the broad CO line wings may appear most prominently in one area of the cloud giving the appearance that the high-velocity flow is localized within the cloud. Elsewhere the broad wings are replaced by one narrow line component arising from the unimpacted region of one of the clouds.

Figure 8 shows model spectra compared with observed  $^{12}\text{CO}$  spectra from BMW. The observed spectra may be understood in light of the model in the following way. The Gaussian peaks arise from the dense cores around the collision zones

near zero systemic velocity. The wings arise from the gas in the original clouds still travelling at a few  $\text{km s}^{-1}$  with respect to the dense core. The most asymmetric profiles such as Figure 8a result from lines of sight off the dense cores where the density difference is not as great. A map of MBM 55 from MBM shows that this spectrum was taken well off the brightness peak as was our modeled spectrum. (The positions of the spectra are listed in the caption to Figure 8 and may be located on the maps in Figs. 4–6.) Maps of MBM 16 and 54 show that the more symmetric spectra in Figures 8b and 8d were observed on the brightness peak. In this case the density contrast between the core and the cloud, and thus the brightness difference between the peak and wings, is quite large.

In comparing the spectra it is important to note that we have not attempted to fit the observed spectra; rather, we have run our models over a very limited range of parameter space, employing for example, only collisions of two identical clouds with average cloud properties. To achieve a CO wing with greater or lesser extent, one could, for example increase or decrease the relative velocities of the colliding clouds. Alternatively, changing the inclination of the relative velocity vector with respect to the line of sight will change the apparent velocities as the cosine of the inclination angle. Similarly, to increase or decrease the ratio of peak line brightness to the wings, one could increase or decrease the density of one of the clouds, or select a model with later or earlier evolution to adjust the ratio of densities in the undisturbed to compressed portions of the clouds. However, given the limited observa-

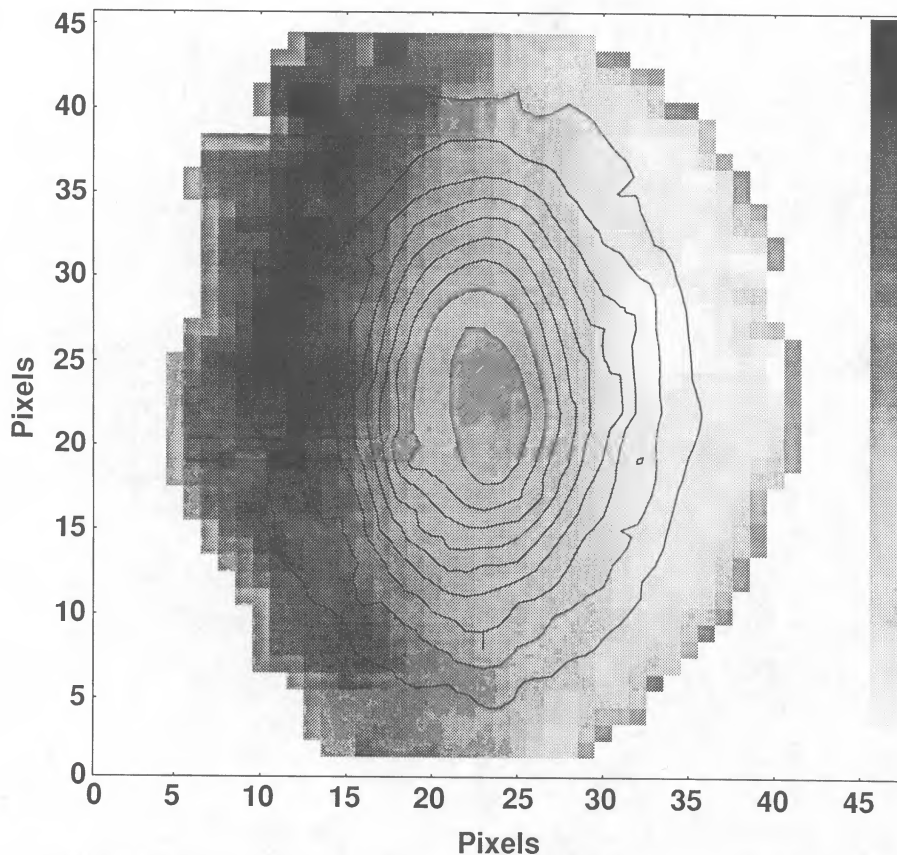


FIG. 4.—Integrated intensity map of model A2 in contour combined with an average velocity map  $\langle v \rangle = \Sigma I v/\Sigma I$  in gray scale. The grid size is 0.046 pc or 1/6 at a distance of 100 pc. The contour interval is 15% of the peak antenna temperature of 0.84 K. The gray scale is linear from  $-1.3$  to  $+1.3 \text{ km s}^{-1}$ , black is positive.

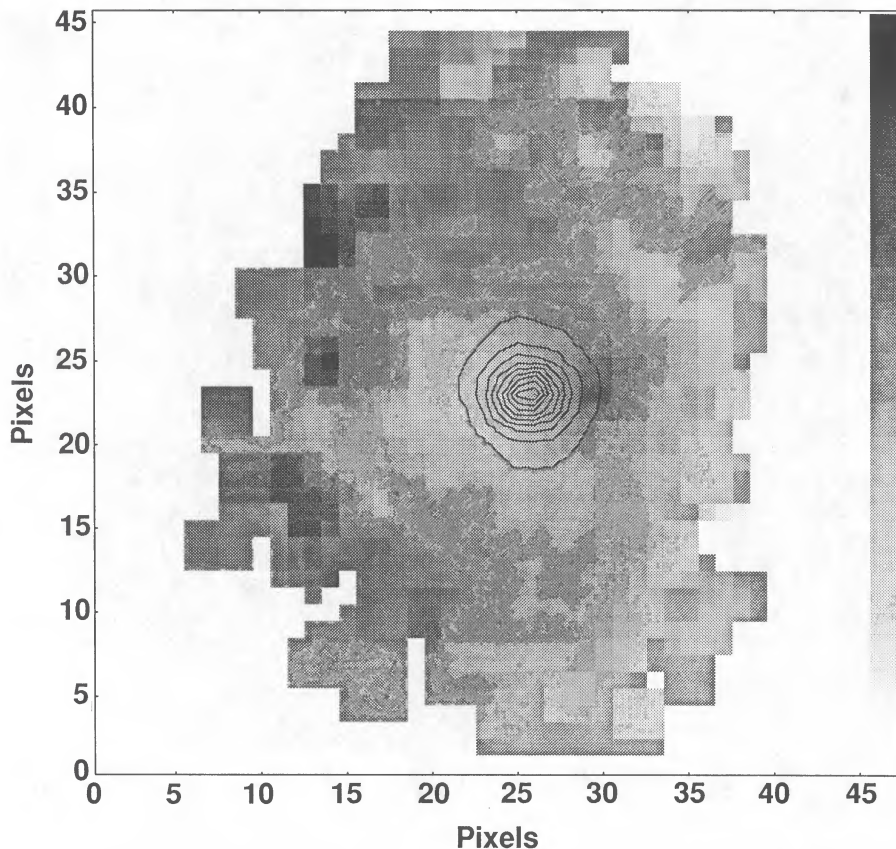


FIG. 5.—Same as Fig. 3, but for model B3. The contour interval is 15% of the peak antenna temperature of 1.2 K. The gray scale is linear from  $-1.6$  to  $+1.4$   $\text{km s}^{-1}$ .

tional data, adjusting the parameters to achieve a closer fit would be a rather arbitrary exercise which would not significantly reduce the uncertainties in the parameters. The computed spectra show that a realistic choice of parameters is capable of matching the observations, without the need for fine-tuning.

## V. DISCUSSION

### a) Implications for Chemistry of High-Latitude Clouds

Observed abundances of OH and  $\text{H}_2\text{CO}$  in high-latitude clouds were found by Magnani, Blitz, and Wouterloot (1988) to be inconsistent with equilibrium models of diffuse cloud chemistry. However, as noted by these authors, the enhanced abundances of these molecules are reproduced in the compressed and heated gas following the passage of a nondissociative shock; see Mitchell and Deveau (1983). Our model suggests that the shocks may result from the collisions between the high-latitude clouds themselves, in contrast to the scenario of Magnani, Blitz, and Wouterloot (1988) that the high-latitude clouds are formed in the compressed gas following a shock in the rarefied ISM. Our model does not preclude this occurrence, and we may investigate this interesting suggestion in the future.

### b) Implications for the Evolution of Giant Molecular Clouds

We briefly speculate on the evolution of a giant molecular cloud complex such as the Rosette Molecular Cloud Complex in light of our model. CO observations by Blitz and Stark

(1986) show the Rosette to be composed of dense clumps,  $M = 500 M_{\odot}$ ,  $n(\text{H}_2) = 250 \text{ cm}^{-3}$ , surrounded by a rarefied intercloud molecular gas of mean density  $n(\text{H}_2) = 2 \text{ cm}^{-3}$ . The intercloud gas is evidenced in these observations again as low-level wings on the CO lines extending to  $\pm 8 \text{ km s}^{-1}$  from the mean VLSR. Our model suggests that cloud collisions will provide a ready source for the diffuse intercloud medium. Our results, plus those of LMPS, show that collisions occurring at large impact parameters will result in the destruction of the colliding clouds. Collisions with small impact parameter will result in a cloud of increased density but considerable ejection of relatively diffuse, high-velocity gas. The higher velocities observed in the Rosette compared with the high-latitude cloud complexes may be caused by the stronger gravitational potential in the more massive complex.

### c) Effect of External Pressure on the Evolution of the High-Latitude Clouds

It is of interest to investigate the fate of a single cloud. As suggested by the ratio  $\alpha = 1.8$ , the cloud was found to expand due to the dominance of the thermal energy over the self-gravity of the cloud. The same occurred when we took  $\Omega = 0$ , indicating that the rotation is only adding to the support and is not its main agent. Clearly our high temperature (80 K) is helping support the cloud, despite the modest external pressure acting to confine the material. A brief attempt was made at constructing an equilibrium cloud (for which we assume an isothermal equation of state). We found that the cloud alterna-

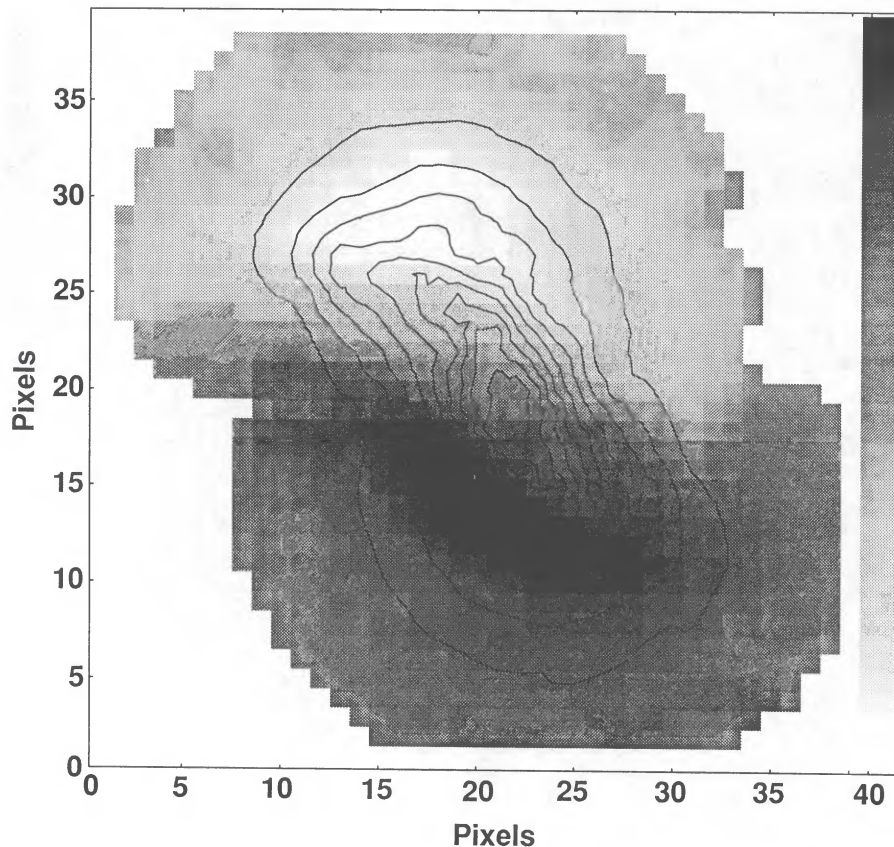


FIG. 6.—Same as Fig. 3, but for model C2. The contour interval is 15% of the peak antenna temperature of 0.42 K. The gray scale is linear from  $-3.4$  to  $+2.6 \text{ km s}^{-1}$ .

tely expanded and contracted, the amplitude of the oscillations decreasing somewhat with each cycle. We believe that “real” high-latitude clouds will be a complex mixture of interacting clouds, including fragments torn apart as a result of collisions. Thus it may be unrealistic to expect each “cloud” to achieve an equilibrium with its surrounds on a relatively short time scale. If it can exist for a few  $t_c$  then it can be identified as a “cloud.” Consequently the effect of an external pressure will be crucial in maintaining the integrity of the “clouds,” which are far from gravitationally bound. This picture is consistent both with theoretical calculations (this paper; LMPS; LH) and the observations (Keto and Myers 1986).

#### d) Collision-induced Star Formation

We found that case 1 resulted in gravitational collapse, despite the fact that in the absence of the collision the clouds will expand into the intercloud medium. This is an important result and shows that for realistic parameters a collision between two high-latitude clouds can induce collapse, presumably with subsequent fragmentation to stellar masses.

To check this result we reran case 1 but with improved resolution, using 25,508 particles. Figure 9 shows  $\log(\rho_{\text{max}}/\rho_0)$  versus time for this run. Note that the configuration clearly exhibits gravitational collapse. Figures 10a, 10c, and 10d show density contours through the center at several times. Figure 10b shows the velocity field at the same time as Figure 10a. Although the expansion along the direction of relative motion is significant, the majority of the mass is collapsing perpendicu-

lar to this direction (through the spheroid). This is reflected in the density contours of the figure, which show the bouncing of the outer boundary, while the center undergoes rapid collapse.

We have seen, however, that a collision between the same clouds but with an impact parameter of  $b = R$  fails to initiate collapse (case 2). It thus appears that for these real clouds, the outcome of a collision depends largely on the impact parameter. For  $b/R$  less than some critical value less than unity, star formation will occur. Presumably the critical ratio will also depend on the relative velocity and mass ratio of the two clouds. We defer to the models of LMPS. Their 2887  $M_\odot$  clouds of 80 K and  $R = 10$  pc have  $\alpha = 1.34$ , which is reasonably close to the value of 1.8 appropriate to the clouds of this paper. LMPS find that, for  $b = 0$ , collapse occurs for  $v_{\text{rel}}/c \leq 8.3$  but not for  $v_{\text{rel}}/c \geq 16.6$ . For  $b/R = 0.5$  collapse occurs for  $v_{\text{rel}}/c \lesssim 4$  but not for  $v_{\text{rel}}/c \gtrsim 4$ . Note that even for  $b = 0$ , however, no collapses are found for  $M_2/M_1 \geq 2.5$ . These results indicate that collisions can indeed induce star formation, but only over a narrow range of  $b \simeq 0$ ,  $M_2 \simeq M_1$ , and  $v_{\text{rel}}/c <$  some critical value depending on various parameters (including  $b$  and  $M_2/M_1$ ). This is consistent with the observed fact that star formation is occurring in some of these high-latitude clouds, but is rare (Keto and Myers 1986; MBM).

#### VI. CONCLUSIONS

1. Broad CO line wings in high-latitude clouds can be reproduced by a model of cloud collisions. The shapes of the wings are produced by a combination of varying density across

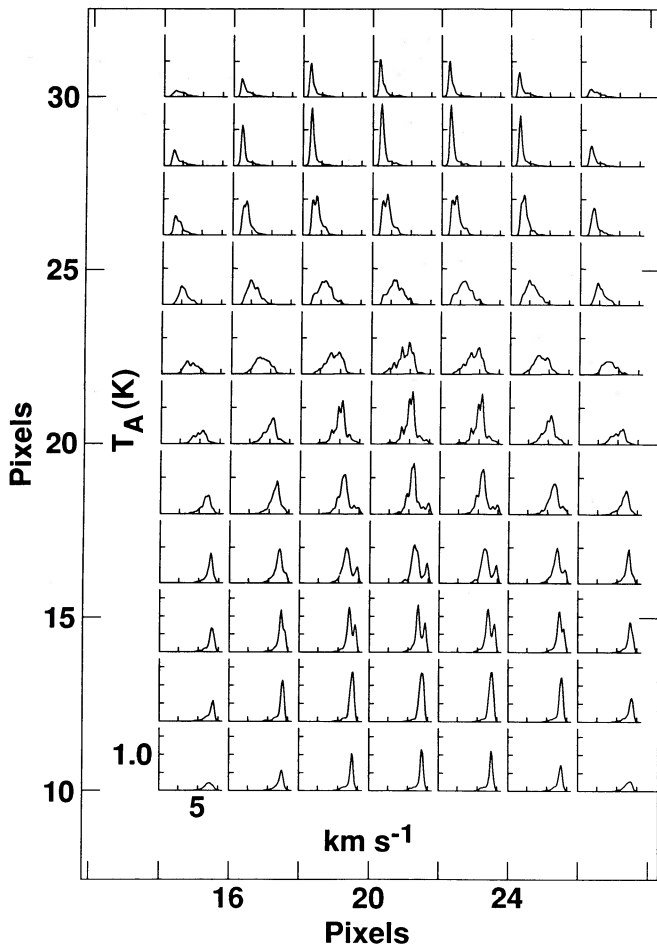


FIG. 7

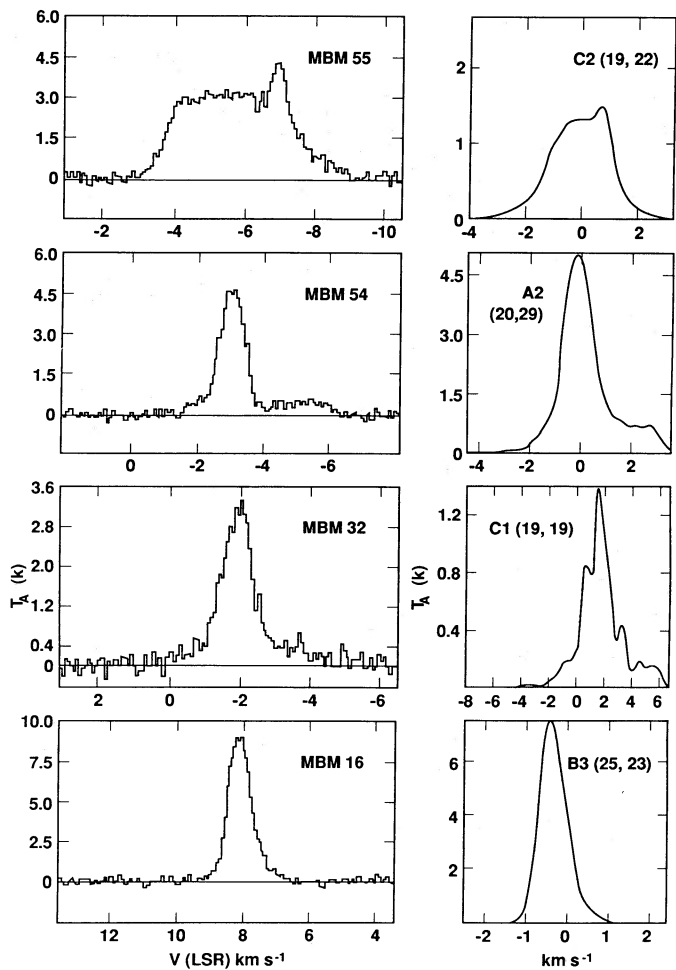


FIG. 8

FIG. 7.—A set of spectra from model C1 in their relative positions across the cloud. The spectra are plotted for every other grid point.

FIG. 8.— $^{12}\text{CO}$  spectra from the observations of MBW (left) with  $^{13}\text{CO}$  spectra from our model showing similar profiles (right). Spectrum *a* is from model C2 at pixel (19, 22), *b* from A2 at (21, 19), *c* from C1 at (19, 19), *d* from B3 at (25, 23).

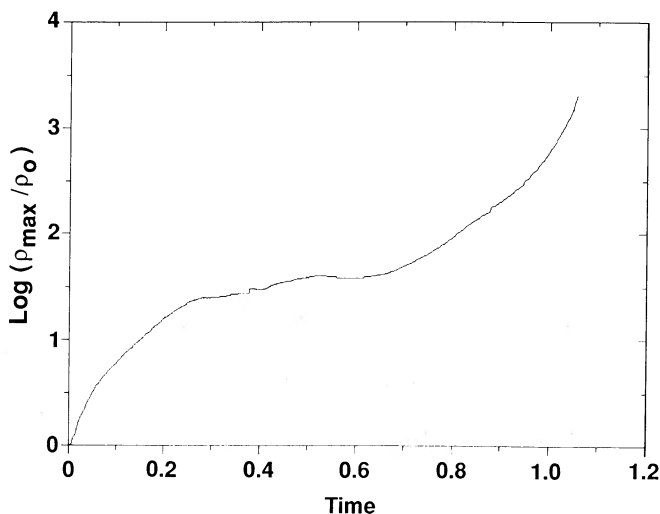


FIG. 9.—Maximum density vs. time for the high-resolution rerun of case 1. The initial density is denoted by  $\rho_0$ . Time is in units of  $t_c$ .

the compressed postcollision cloud, the bulk motion of the two initial clouds, and projection effects.

2. Cloud collisions can induce rapid gravitational collapse in initially stable clouds. Indications are that the two clouds must have nearly equal mass, and nearly zero impact parameter, for the cloud parameters used in this paper.

3. For the typical high-latitude cloud with  $M \leq 100 M_\odot$ ,  $R \approx 1\text{--}2$  pc and  $\log n \leq 3 \text{ cm}^{-3}$ , the external pressure of the H I or molecular intercloud medium plays a significant role in defining the structure and in confining the cloud.

The authors gratefully acknowledge W. J. Welch for providing a subroutine to compute the CO rate matrix, R. N. Henriksen for suggesting this topic, and N. Mackanic of the National Magnetic Fusion Energy Computer Center for cheerful technical assistance. Work performed under the auspices of US Department of Energy at Lawrence Livermore National Laboratory under contract No. W-7405-ENG-48.

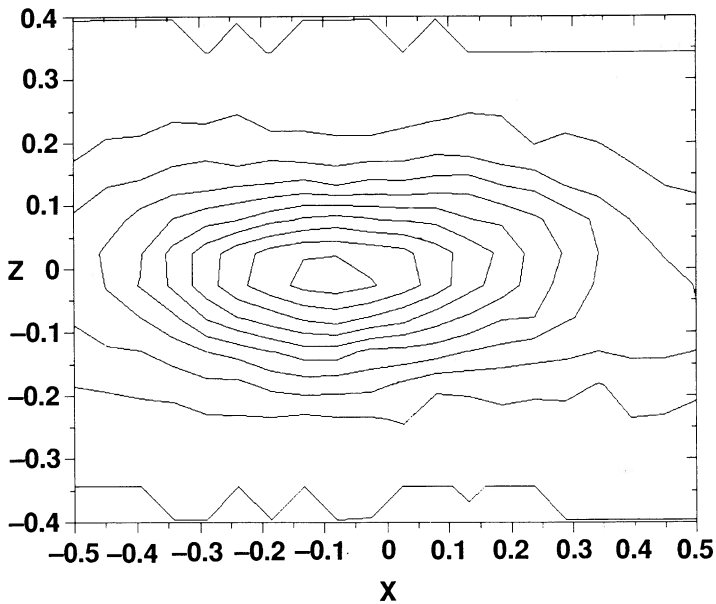


FIG. 10a

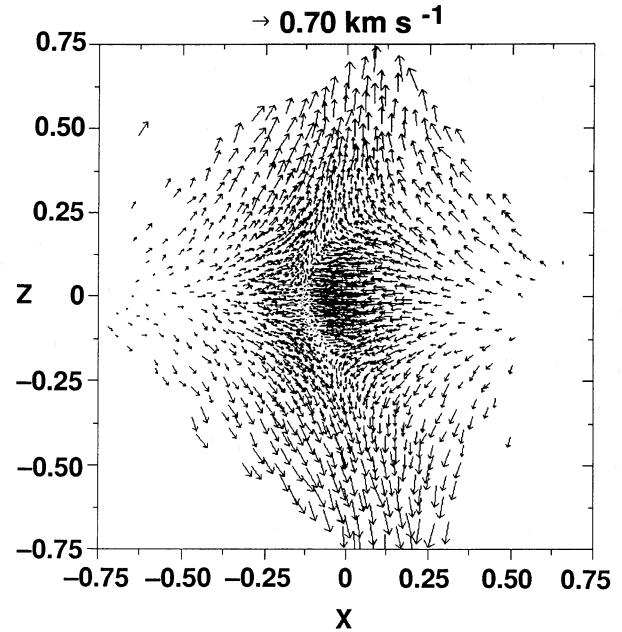


FIG. 10b

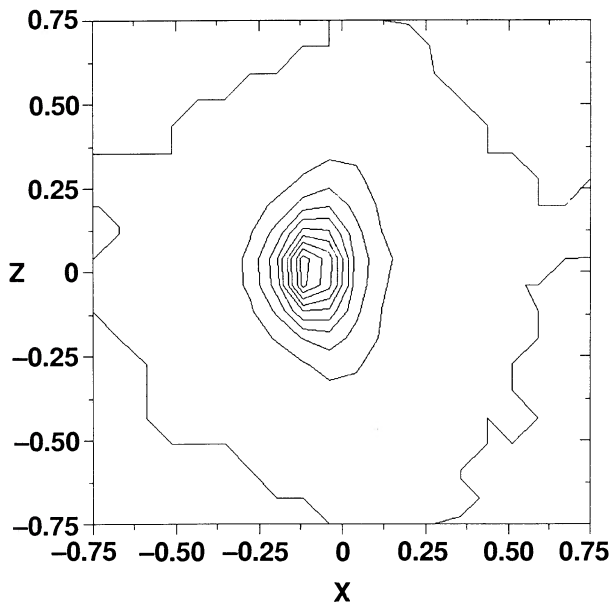


FIG. 10c

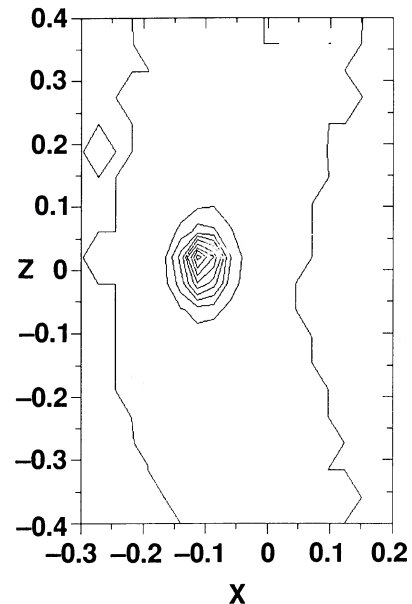


FIG. 10d

FIG. 10.—Density contours and velocity field in the  $x, z$  plane through the cloud center for the high-resolution rerun of case 1. (a) For a time of  $0.672t_c$ , when  $h = 0.032$ . Contour level is  $5.67 \times 10^{-21} \text{ g cm}^{-3}$ . (b-c) For  $t = 0.890t_c$ , when  $h = 0.024$ . Contour level in (c) is  $2.10 \times 10^{-20} \text{ g cm}^{-3}$ . (d)  $t = 1.057t_c$ , when  $h = 0.012$ . Contour level is  $2.23 \times 10^{-19} \text{ g cm}^{-3}$ .

## REFERENCES

- Blitz, L., and Stark, A. A. 1986, *Ap. J. (Letters)*, **300**, L89.  
 Blitz, L., Magnani, L., and Wandel, A. 1988, preprint (BMW).  
 de Vries, H. L., Heithausen, A., and Thaddeus, P. 1987, *Ap. J.*, **319**, 723.  
 Elmegreen, B. G. 1988, *Ap. J.*, **326**, 616.  
 Goldstein, H. 1972, *Classical Mechanics* (New York: Addison-Wesley).  
 Keto, E. R. 1989, *Ap. J.*, submitted.  
 Keto, E. R., and Myers, P. C. 1986, *Ap. J.*, **304**, 466.  
 Lattanzio, J. C., and Henriksen, R. N. 1988, *M.N.R.A.S.*, **232**, 565 (LH).  
 Lattanzio, J. C., and Monaghan, J. J. 1989, in preparation.  
 Lattanzio, J. C., Monaghan, J. J., Pongracic, H., and Schwarz, M. P. 1985, *M.N.R.A.S.*, **215**, 125 (LMPS).  
 Magnani, L., Blitz, L., Carpenter, J. M., Kassim, N. E., and Nath, B. 1989, in preparation.  
 Magnani, L., Blitz, L., and Mundy, L. 1985, *Ap. J.*, **295**, 402 (MBM).  
 Magnani, L., Blitz, L., and Wouterloot, J. G. A. 1988, *Ap. J.*, **326**, 909.  
 Monaghan, J. J., and Lattanzio, J. C. 1985, *Astr. Ap.*, **149**, 135.  
 Monaghan, J. J., and Varnas, S. R. 1988, *M.N.R.A.S.*, **231**, 515.

E. R. KETO and J. C. LATTANZIO: Institute of Geophysics and Planetary Physics, Lawrence Livermore National Laboratory, POB 808-L413, Livermore, CA 94550